A&A 503, 259–264 (2009)
DOI: 10.1051/0004-6361/200912080

Astronomy & Astrophysics

Statistical analysis of micrometeoroids flux on Mercury

P. Borin[1,2], G. Cremonese[2], F. Marzari[3], M. Bruno[4], and S. Marchi[5]

[1] CISAS, University of Padova, via Venezia 15, 35131 Padova, Italy
e-mail: patrizia.borin@unipd.it
[2] INAF – Astronomical Observatory of Padova, Vicolo dell'Osservatorio 5, 35131 Padova, Italy
e-mail: gabriele.cremonese@oapd.inaf.it
[3] Department of Physics, via Marzolo 8, 35131 Padova, Italy
e-mail: marzari@pd.infn.it
[4] Department of Mineralogical and Petrological Science, via Valperga Caluso 35, 10125 Torino, Italy
e-mail: marco.bruno@unito.it
[5] Department of Astronomy, Vicolo ell'Osservatorio 5, 35131 Padova, Italy
e-mail: simone.marchi@unipd.it

Received 16 March 2009 / Accepted 21 May 2009

ABSTRACT

Context. Meteoroid impacts are an important source of neutral atoms in the exosphere of Mercury. Impacting particles of size smaller than 1 cm have been proposed to be the major contribution to exospheric gases. However, our knowledge of the fluxes and impact velocities of different sizes is based on old extrapolations of similar quantities on Earth.
Aims. We compute by means of N-body numerical integrations the orbital evolution of a large number of dust particles supposedly produced in the Main Belt. They migrate inward under the effect of drag forces until they encounter a terrestrial planet or eventually fall into the Sun. From our numerical simulations, we compute the flux of particles hitting Mercury's surface and the corresponding distribution of impact velocities.
Methods. The orbital evolution of dust particles of different sizes is computed with a numerical code based on a physical model developed previously by Marzari & Vanzani (1994, A&A, 283, 275). It includes the effects of Poynting-Robertson drag, solar wind drag, and planetary perturbations. A precise calibration of the particle flux on Mercury has been performed by comparing our model predictions for dust infall on to Earth with observational data.
Results. We provide predictions of the flux to different size particles impacting Mercury and their collisional velocity distribution. We compare our results with previous estimates and we find that these collisional velocities are lower but that the fluxes are significantly higher.

Key words. methods: N-body simulations – methods: statistical – meteors, meteoroids – planets and satellites: individual: Mercury

1. Introduction

The major sources of the dust population in the inner Solar System are asteroid collisions and debris released by short-period comets. The comminution products of cratering and fragmentation events in the asteroid belt are the origin of dust bands observed in IRAS data (Low et al. 1984; Hauser et al. 1984). These bands were interpreted as dust produced by the continuous collisional activity of the asteroid, which provides a constant supply of debris (Dermott et al. 1984; Sykes & Greenberg 1986). The dust grains produced in the asteroid belt slowly evolve under solar radiation forces and the gravitational force of the Sun and planets. In particular, particles smaller than 1 cm are significantly perturbed by Poynting-Robertson and solar wind drag and spiral towards the Sun on timescales that depend on their size and composition. During their journey, they may be not only gravitationally scattered by terrestrial planets but also trapped into one or more mean motion resonances (Jackson & Zook 1992; Marzari & Vanzani 1994; Marzari et al. 1996). Because of the interplay between the gravitational perturbations of the planets and the Poynting-Robertson drag, the orbital evolution can be quite complex. As a consequence, models based on a uniform and steady flux of dust grains from the Main Belt into the inner regions of the Solar System may be inappropriate. A full numerical approach is required to estimate how the grain population evolves while approaching the Sun.

Meteoroid impacts have a very important role in the evolution of Mercury's surface and exosphere. Since the exobase is presently at the surface of the planet, the exosphere sources and sinks are tightly linked to the composition and structure of the planet surface. A significant fraction of volatiles released into the exosphere is thought to be produced by impact vaporization of meteoritic material on the surface (Cremonese et al. 2005). We may be able to identify two population of meteoroids depending on their dynamical evolution: small particles ($r < 1$ cm) dominated by the Poynting-Robertson drag, and large particles ($r > 1$ cm) driven by gravity only.

In this paper, we study the long-term evolution of dust grains (i.e., $r < 1$ cm) from the Main Belt to Mercury. By means of numerical simulations, we estimate the flux of dust particles on the surface of Mercury and their impact velocity distribution. The overall flux is tuned on the basis of direct measurements of the mass accretion rate of cosmic dust at Earth orbit from Long Duration Exposure Facility (LDEF) satellite (Love & Brownlee 1993). According to Dermott et al. (2002), all the dust collected from satellite LDEF (Love & Brownlee 1993) originates in typical asteroidal orbits. These authors show that they can explain

the measured accretion mass rate with that coming from the zodiacal dust bands. The major contributions to these bands are asteroidal collisions (about 48%) and short period comet dust production. The grains produced by short period comets by the time they reach the Earth may approach the planet with the low velocities typical of asteroidal orbits (Liou & Zook 1996). These grains are trapped in mean motion resonances with Jupiter and their eccentricities and inclinations are damped by the time they encounter the Earth. Following Dermott et al. (2002), about 34% of the dust reaching Earth might be resonant cometary dust. As a consequence, independently of the source, most of the interplanetary dust particles might indeed encounter the Earth on low eccentricity and low inclination orbits.

A model of dust originating in comets claims that a fraction as high as 90% of the dust collected at the Earth surface might be of cometary origin (Wiegert et al. 2009). However, this result strongly depends on the size distribution adopted for the dust particles ejected from comets. They calibrate the flux only for high speed large meteroid impacts on Earth and propagate the results to small dust sizes. We do not enter this debate in this paper. Our approach is purely dynamical and we consider dust reaching the Earth on asteroidal orbits, independently of its source. As a consequence, we account for a significant contribution of dust at the Earth. When future experiments are able to measure the impact velocity on dust collection facilities, it will be possible to discriminate between dust particles on low velocity asteroidal orbits and those on high velocity cometary trajectories. The flux of dust measured, such as that obtained by LDEF (Love & Brownlee 1993), should then consist of two components depending on the impact velocity: one that originated in low eccentricity and low inclination orbits (either coming from the asteroid belt or from short period comets), and one from cometary trajectories. A tuning coefficient can be derived in this scenario that can be applied to our results concerning the fraction of grains that approach the Earth at low relative velocity. This fraction is propagated to Mercury in our model.

2. Dynamical evolution model

To estimate the meteoritic flux at the heliocentric distance of Mercury, we utilize the dynamical evolution model of dust particles of Marzari & Vanzani (1994). It numerically integrates a $(N+1)+M$ body problem (Sun + N planets + M body with negligible mass) with the high-precision integrator RA15. Radiation and solar wind pressure and Poynting-Robertson drag are included as perturbative forces together with the gravitational attractions of all the planets in the Solar System.

Adopting the same formalism as Marzari & Vanzani (1994), the gravitational term is given by

$$\boldsymbol{F}_{\rm gra} = \boldsymbol{F}^{\rm k} + \boldsymbol{F}^{\rm d} + \boldsymbol{F}^{\rm ind}, \tag{1}$$

where $\boldsymbol{F}^{k}$ is the Keplerian force, $\boldsymbol{F}^{\rm d}$ is the direct force, and $\boldsymbol{F}^{\rm ind}$ is the indirect force. Equation (1) can be written as

$$\boldsymbol{F}_{\rm gra} = \frac{Gm(M_{\rm Sun}+m)\boldsymbol{r}_{\rm Sun}}{r_{\rm Sun}^3} + \frac{Gm\sum_{j=1}^{N} m_j \boldsymbol{r}_j}{r_j^3} + \frac{Gm\sum_{j=1}^{N} m_j \boldsymbol{r}_{{\rm Sun},j}}{r_{{\rm Sun},j}^3}, \tag{2}$$

where $r_{\rm Sun}$ is the distance between the Sun and dust particles, r_j is the distance between planets and dust particles, m is the mass of dust particles, and N is the number of planets.

The non-gravitational term consists of two terms: the radiation force, $\boldsymbol{F}_{\rm rad}$ and the force given by the solar wind, $\boldsymbol{F}_{\rm wnd}$,

$$\boldsymbol{F}_{\rm ngra} = \boldsymbol{F}_{\rm rad} + \boldsymbol{F}_{\rm wnd}, \tag{3}$$

where

$$\boldsymbol{F}_{\rm rad} = \frac{S}{c}\left(1-\frac{\dot{r}}{c}\right)AQ_{\rm pr}\hat{\boldsymbol{p}} = f_{\rm r}\hat{\boldsymbol{p}}, \tag{4}$$

and

$$\boldsymbol{F}_{\rm wnd} = \sum_j \frac{\eta_j u^2}{2} AC_{{\rm D},j}\hat{\boldsymbol{u}} = f_w\hat{\boldsymbol{u}}. \tag{5}$$

Where, $\hat{\boldsymbol{p}} = \frac{\boldsymbol{c}-\boldsymbol{v}}{c}$, $\boldsymbol{c}$ is the velocity of the light (in the anti-solar direction) and $\boldsymbol{v}$ is the orbital velocity of the dust particle, and $\hat{\boldsymbol{u}} = \frac{\boldsymbol{u}}{u}$ with $\boldsymbol{u} = \boldsymbol{w}-\boldsymbol{v}$, where $\boldsymbol{w}$ is the solar wind flow bulk velocity in the average phase (Mukai et al. 1982; Marzari & Vanzani 1994); the spatial mass density of the component j of the solar wind flow is given by $\eta_j = n_j m_j$ for mass m_j and number density n_j; A is the geometrical cross section of the grain; $Q_{\rm pr}$ is the dimensionless radiation-pressure coefficient averaged over the solar spectrum; $C_{{\rm D},j}$ is the dimensionless drag coefficient due to the j-component of the wind flow; S is the solar radiation flux density at heliocentric distance r, and we can write $S = S_0(\frac{r_0}{r})^2$; $w_0 \simeq 4\times10^7$ cm/s for w at 1 AU; and $\eta_{p,0}+\eta_{\alpha,0} \simeq 1.2\eta_{p,0}$ (Marzari & Vanzani 1994).

The efficiency of the radiation and corpuscolar resistive forces can be expressed by defining their ratio with respect to the solar gravity in the following manner:

$$\beta_{\rm r} = \frac{f_{\rm r}}{f_{\rm g}}\left[\frac{c}{c-\dot{r}}\right] = \left(\frac{SAQ_{\rm pr}}{c}\right)\cdot\left(\frac{GM_\odot m}{r^2}\right)^{-1}, \tag{6}$$

and

$$\beta_w = \frac{f_{\rm w}}{f_{\rm g}}\left[\frac{w}{|\boldsymbol{w}-\boldsymbol{v}|}\right] = \left(\frac{f_{w0}\psi}{\kappa}\right)\cdot\left(\frac{GM_\odot m}{r^2}\right)^{-1}, \tag{7}$$

for $\kappa = \frac{u}{w}$ and $\psi = \frac{f_w}{f_{w0}}$, where f_{w0} is obtained from f_w when neglecting the velocity dispersion of wind particles and taking no notice of the contribution of momentum carried away by the sputtered molecules to $\boldsymbol{F}_{\rm wnd}$.

Taking the reference-distance r_0 to be equal to 1 AU and assuming a dust particle of spherical shape of radius s, one obtains

$$\beta_r = \frac{3S_0 r_0^2}{4GM_\odot c}\frac{Q_{\rm pr}}{\varrho s} = 5.74\times10^{-5}\frac{Q_{\rm pr}}{\varrho s}, \tag{8}$$

and

$$\beta_w = \frac{3(\eta_{p,0}+\eta_{\alpha,0})r_0^2 w_0^2}{4GM_\odot}\frac{\psi\kappa}{\varrho s} \simeq 3.27\times10^{-8}\frac{\psi\kappa}{\varrho s}, \tag{9}$$

where ϱ is the mass density of the dust particle measured, such s, in cgs units (Marzari & Vanzani 1994).

Finally, the relative importance of the radiation and corpuscolar forces can be estimated by the parameter

$$\gamma = \frac{\beta_w}{\beta_r} \simeq 5.7\times10^{-4}\frac{\psi\kappa}{Q_{\rm pr}}\cdot \tag{10}$$

The adopted numerical algorithm for solving the equations of motion is the RA15 version of the RADAU integrator by Everhart (1985). The choice of this integrator is dictated by the frequent occurrence of close encounters between dust particles

and planets. In this case, RA15 is very precise since it uses a variable stepsize.

Our simulations start with a ring of 1000 particles. The initial semi-major axis is randomly selected to be in between 2.1 and 3.3 AU, the initial eccentricity varies in the range 0.0–0.4, and the inclination in the range 0–20°. This choice reflects the average orbital elements of asteroids assumed to be the sources of the dust ring. For the grains, we assume a density of 2.5 g cm^{-3}, a reasonable value for dust particles originating in the Main Belt (Grün et al. 1985). Spherical particles are considered in terms of the approximation of Mie's theory for which $Q_{\rm pr}$, the dimensionless radiation-pressure coefficient averaged over the solar spectrum, is 0.53 (Marzari & Vanzani 1994; Mukai et al. 1982).

3. Flux estimate from numerical integration

We compute the orbital evolution of the dust ring until all the particles move well inside the orbit of Mercury. To estimate the flux of impacting grains, we use a statistical approach since the number of computed impacts is negligible. Any time a dust grain falls within ten times the influence sphere of Mercury, we record the minimum approach distance and the grain-planet relative velocity. At the end of the run, we have a list of close encounters that we can statistically analyse. We divide the encounters in bins of radial distance from the planet centre and we perform a least squares fit to the data with a parabola function as P_0R^2. The least squares fit, performed by assuming a standard deviation for each data bin of $\sqrt{N_i}$ (where N_i is the number of close encounters in each bin), allows us to compute the parameter P_0 (Marzari et al. 1996). At this point, if we use R to represent the radius of Mercury, we derive the fractional number of impacts on the surface of the planet $n_{\rm M}$. We take proper account of the gravitational focusing factor caused by Mercury's attraction. The relative velocity distribution is instead well approximated by that computed for each close encounter properly corrected for the gravitational focusing factor. With 1000 particles, we can study reasonably well the dynamical behaviour of the real grains as they approach the planet. From the number of impacts $n_{\rm M}$, we can estimate the flux $g_{\rm M}$ by dividing $n_{\rm M}$ by an effective time interval ΔT over which the impacts occur. In our simulations, the distribution of close encounters versus time exhibits a rapid growth as the first grains of the ring begin to approach the planet. The distribution reaches a plateau where the rate of encounters is approximately constant, and finally it rapidly declines. We define an effective time interval ΔT by inspecting the distribution of encounters with time, where ΔT represents the timespan during which the encounter rate is approximately constant. The flux $g_{\rm M}$ on the planet is then estimated to be the number of impacts $n'_{\rm M}$ (rescaled to account for encounters occurring only during ΔT) divided by ΔT.

In our simulations, we do not consider particles of radius smaller than 1 μm because, in general, solar radiation pressure reduces solar gravity sufficiently to drive these particles out of the Solar System (they become beta meteoroids). In other words, the Poynting-Robertson and the solar gravity no longer dominate (Burns et al. 1979; Sykes et al. 2004).

4. Calibration of flux

To calibrate our flux, i.e., to compute the true number of grains represented by our 1000 test particles, we need to know the density of particles within our initial ring. In the literature, the particle density in the Main Belt for different particle sizes is not clearly defined. It is given by a relation between the number of particles and their size only for the IRAS dust band, which is not applicable to the entire Main Belt (Mann et al. 1996).

A more robust way is to calibrate the density of our initial dust ring by means of the observed flux of grains on the Earth. For this purpose, during each simulation we record the close encounters between test particles and the Earth. As for Mercury, we then extrapolate the flux $g_{\rm E}(r)$ of particles of a given size r on the Earth surface. We then derive a set of calibration coefficients $C(r)$ for all the sizes we considered in our simulations given by $C(r) = g_{\rm M}(r)/g_{\rm E}(r)$. These coefficients represent the change in the flux of equal size particles as they move from the Earth to Mercury and they account for the dynamical behaviour of the dust grains (e.g., resonances, close encounters with the planets, and acceleration of migration due to eccentricity stirring). These coefficients are used to "transport" the curve of the Earth meteoroid flux given by Love & Brownlee (1993), which was obtained from experimental data taken by the satellite LDEF, to Mercury. The flux on Mercury is calculated by interpolating a curve for the mass flux, similar to that of Love & Brownlee (1993), that is constrained to reproduce the scaled points computed by multiplying the Love & Brownlee (1993) curve by the $C(r)$s.

Additional effort is needed before rescaling the flux of Love & Brownlee (1993) to Mercury. In their paper, Love and Brownlee adopted an average meteoroid speed of 16.9 km s^{-1} to compute the flux values, while in our dynamical model we obtain a mean velocity of 18.6 km s^{-1} for grains coming from the Main Belt and impacting the Earth. Following the same method as Love & Brownlee (1993), we computed a new value of flux with our average velocity. Figure 1 shows the fluxes calculated with the two different average velocities. A slightly lower value of flux is obtained with the higher impact velocity.

It is important to note that Love and Brownlee determined the mass flux and size distribution of micrometeoroids in the submillimiter size range, in particular the mass range 10^{-9} to 10^{-4} grams, by measuring hypervelocity impact craters found on the space-facing end of the gravity-gradient-stabilized LDEF satellite. They found that the total mass accreted by the Earth per year across the size range sampled in their work is $(40 \pm 20) \times 10^6$ kg/year. The major source of uncertainty is the value of the encounter velocity. Dermott et al. (2002) interpreted the mass accretion rate on the Earth as being caused by particles in the zodiacal cloud on typical asteroidal orbits. The possibility that in the flux there is a consistent component on cometary highly eccentric and inclined orbits (Wiegert et al. 2009) can be taken into account in our model with an additional tuning factor that indicates the fraction of dust coming from the two different types of orbits.

5. Impact velocity

An important aspect of the model of Cintala (1992) for computing the flux of meteoroids on Mercury is the velocity distribution of impacting particles. The differential flux is written as

$$\Phi(v, m) = f(v) \cdot h(m), \tag{11}$$

where $f(v)$ is the velocity distribution of dust particles (s/km), and $h(m)$ is the mass distribution function of the impacting particles (g^{-1} cm^{-2} s^{-1}).

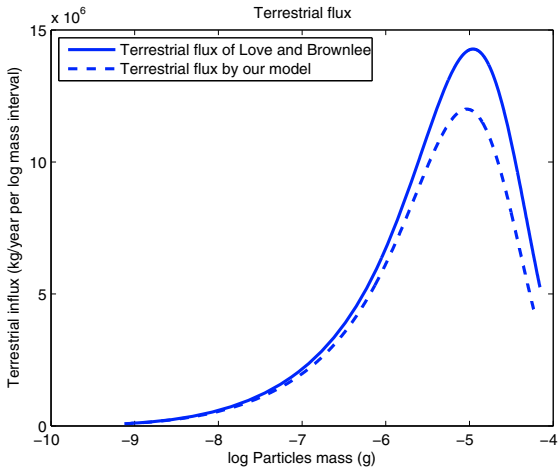

Fig. 1. Terrestrial flux calculated following the Love and Brownlee procedure using the two differen average velocities of 16.9 km s^{-1} and 18.6 km s^{-1}.

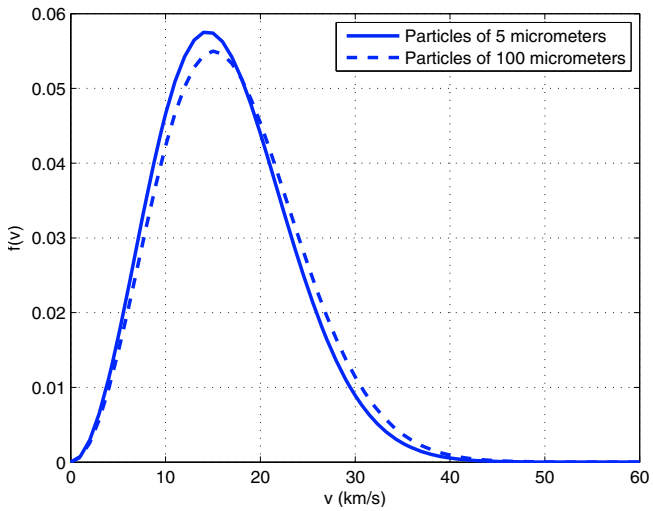

Fig. 2. Velocity distribution function of particles with radius of 5 μm and 100 μm.

The velocity distribution function is given by the following equation

$$f(v) = kr^{1.5}\left[\frac{v}{\sqrt{r(v^2 - v_{\rm Me}^2) + v_{\rm Ee}^2}}\right]^3 e^{\left(-\xi\sqrt{r(v^2-v_{\rm Me}^2)+v_{\rm Ee}^2}\right)}, \qquad (12)$$

where $k = 3.81$, $\xi = 0.247$ are constant, $r = 0.387$ AU is the mean distance of Mercury from the Sun, v is the impact velocity of dust particles on Mercury, $v_{\rm Ee} = 11.1$ km s^{-1} is the escape velocity for the Earth at 100 km altitude, and $v_{\rm Me} = 4.25$ km s^{-1} is the escape velocity at the surface of Mercury. This velocity distribution is derived based on the assumption that the dust density is constant between the Earth and Mercury. However, according to Leinert et al. (1981), the dust density of the grains increases as $r^{-1.3}$ and Eq. (12) at Mercury becomes

$$f(v) = kr^{0.2}\left[\frac{v}{\sqrt{r(v^2 - v_{\rm Me}^2) + v_{\rm Ee}^2}}\right]^3 e^{\left(-\xi\sqrt{r(v^2-v_{\rm Me}^2)+v_{\rm Ee}^2}\right)}, \qquad (13)$$

With our approach, the distribution of impact velocities is a direct outcome of the code. It is directly related to the dynamical behavior of the particles as they approach Mercury and accounts for the interplay between non-gravitational forces, resonances, and planet scattering.

In Fig. 2, we compare the velocity distribution for particles of 5 μm and 100 μm, respectively. There is no substantial difference between the two curves and this is also true for all the other particle sizes that we considered in our simulations (5, 10, 20, 30, 40, 50, 60, 70, 80, 90, 100 μm). As a consequence, we combine all the data for the relative velocity in a single normalized distribution that can be compared to that of Cintala (1992). This is shown in Fig. 3. It is noteworthy that the analytic velocity distribution of Cintala (1992) is shifted towards the high velocity tail and its peak is slightly higher than that obtained from our numerical distribution. Our average impact velocity at Mercury is 16.81 km s^{-1}, while that predicted by the Cintala (1992) model is 20.50 km s^{-1}, about 18.0% higher.

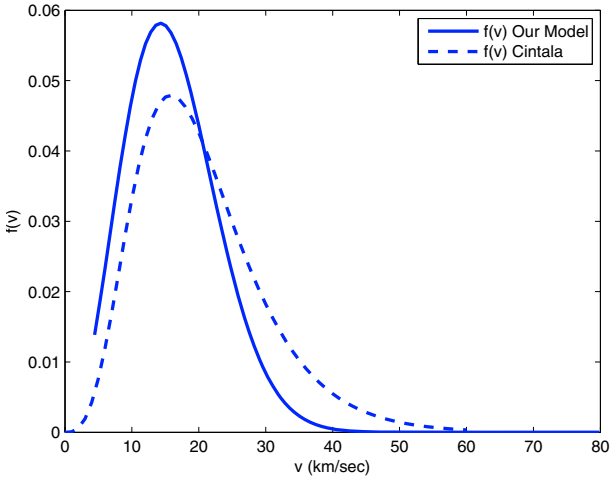

Fig. 3. Comparison of velocity distribution given by our model and Cintala's model.

6. Micrometeoroid flux on Mercury

According to the approach described in Cintala (1992), the impact flux depends on both the velocity distribution of dust particles and their mass distribution function.

The Cintala's mass distribution reported in Eq. (11) is

$$h(m) = -\frac{1}{mF_1}\exp\left(\sum_{i=0}^{11} c_i \ln(m)^i\right)\cdot\left[\sum_{i=1}^{11} i\cdot c_i \ln(m)^{i-1}\right], \qquad (14)$$

where m is the projectile mass, $F_1 = 0.364$, c_i are constants (Cintala 1992; Cremonese et al. 2005).

The advantage of our numerical approach is that we do not need to make any assumption about the density or velocity distribution since they are computed directly from the particle dynamics. After the calibration at the Earth's orbit, we follow the evolution of the particle ring as it reaches Mercury. Both the particle density and velocity distributions are derived properly from the numerical data once statistically interpreted. We directly compute the flux $g_{\rm M}$ for any particle size without any a priori assumption about the density evolution.

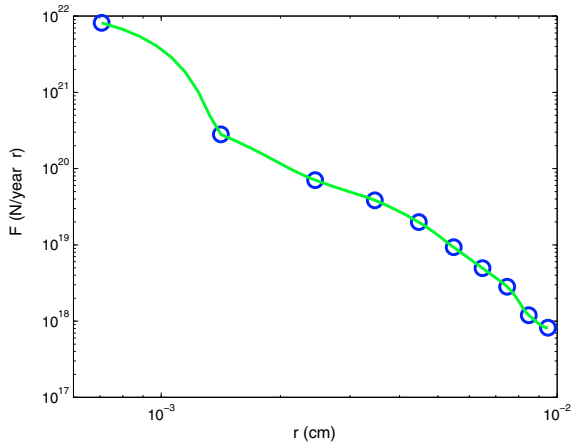

Fig. 4. Flux on Mercury obtained with our numerical simulations (blue points) and the cubic spline curve (green line).

Table 1. Flux obtained by Cintala and our model in the range 5–100 μm.

Model	$\frac{N}{\text{year}}$	$\frac{\text{g}}{\text{cm}^2\cdot\text{s}}$
Cintala's model	4.073×10^{16}	1.402×10^{-16}
Our's model	3.104×10^{18}	2.382×10^{-14}

The data for the flux $g_{\rm M}$ of each particle size were interpolated to obtain an analytical curve. In Fig. 4, we show an interpolation of the numerical fluxes $g_{\rm M}$. By integrating the analytical function, we estimate the total flux in the size range that we considered, which can be compared with that given by Cintala (1992) (see Table 1).

Table 1 shows that the total number of impacts given by Cintala, measured in N/year, is about 76 times lower than our estimate, and that our mass flux estimate given in $g/(\text{cm}^2 \times \text{s})$ is 170 times higher.

7. Lifetime and resonances

Before impacting Mercury the lifetime of dust particle strongly depends on their radius and mass. In our simulations, we find that the lifetime of dust grains increases with their radius and this is a consequence of both a slower drift rate caused by P-R drag and resonance trapping. However, the lifetime is not a trivial linear function of the size since the interplay between planet scattering and resonances strongly affect the eccentricity, which is relevant in determining the drift rate produced by the P-R drag. In Figs. 5 and 6, we show some examples of resonance trapping for different size particles. During the resonant evolution it is noteworthy that the eccentricity of the particle increases leading to a much faster orbital decay once out of the resonance. Large particles are trapped more frequently and their eccentricity is, as a consequence, often increased accelerating their migration towards Mercury. Accounting for all these dynamical effects is possible only with a full numerical approach.

8. Conclusions

In this paper, we have analysed the dynamical evolution of micrometeoroids from the Main Belt to Mercury to compute the flux of meteoroids on the surface of the planet. In our numerical model, we include the gravitational perturbations of all the planets and the Poynting-Robertson drag. From the data of the simulations, we extrapolate the ratios of dust grain fluxes on Earth and Mercury for different particle sizes. These ratios are used to "transport" the experimental curve of Love & Brownlee (1993) for the mass flux on the Earth to Mercury accounting for all the dynamical effects such as resonance trapping, planet scattering, and eccentricity excitation.

Our results for the flux of micrometeoroids in terms of mass is about 170 times higher than previous estimates (Cintala 1992). The flux computation depends on the calibration of the dust flux at the Earth orbit. This is performed on the basis of the LDEF satellite data that are interpreted as being determined mostly by dust grains on asteroidal orbits. This accounts for particles either coming from asteroids or short period comets (Dermott et al. 2002). The possibility that a significant fraction of dust comes from typical cometary orbits can be accounted for with an additional tuning coefficient. This will be possible when data on the dust impact velocities become available.

The flux estimate is a relevant parameter for calculating the contribution of neutral atoms to the exosphere (Cremonese et al. 2005) and for the definition of the environment of Mercury in view of future space missions such as the ESA-JAXA BepiColombo.

Acknowledgements. We wish to thank M. Fulle for his advices.

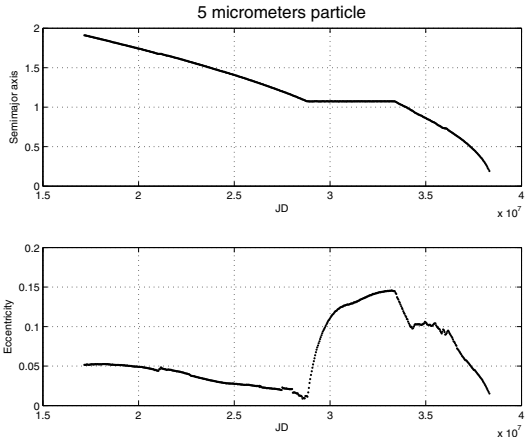

Fig. 5. Semimajor axis and eccentricity for a particle of 5 μm of radius.

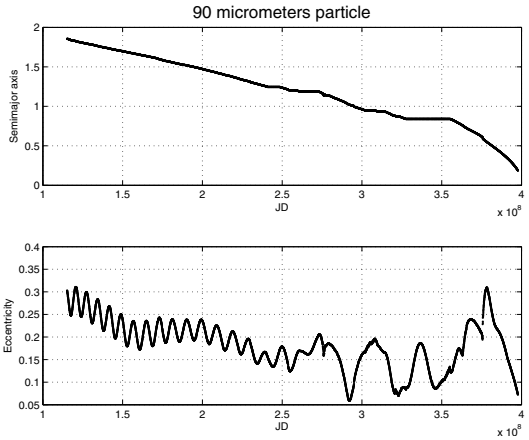

Fig. 6. Semimajor axis and eccentricity for a particle of 90 μm of radius.

References

Burns, J. A., Lamy, P. L., & Soter, S. 1979, Icarus, 40, 1
Cintala, M. J. 1992, J. Geophys. Res., 97
Cremonese, G., Bruno, M., Mangano, V., et al. 2005, Icarus, 177, 122
Dermott, S. F., Nicholson, P. D., & Burns, J. A. 1984, Nature, 312, 505
Dermott, S. F., Durda, D. D., Grogan, K., et al. 2002, Asteroidal dust, in Asteroids III, ed. C. C. Bottke, B. Paolicchi (Arizona: University Press)
Everhart, E. 1985, Dynamics of Comets: Their Origin and Evolution, Proc. IAU Coll. 83, 185
Grün, E., Zook, H. A., Fechtig, H., et al. 1985, Icarus, 62, 244
Hauser, M. G., Gillett, F. C., Low, F. J., et al. 1984, ApJ, 278, L15
Jackson, A. A., & Zook, H. A. 1992, Icarus, 97, 70
Leinert, C., Richter, I., Pitz, E., et al. 1981, A&A, 103, 177
Liou, J. C., & Kook, H. A. 1996, Icarus, 23, 491
Love, S. G., & Brownlee, D. E. 1993, Science, 262
Low, F. J., Young, E., Beintema, D. A., et al. 1984, ApJ, 278, L19
Mann, I. 2004, Space Sci. Rev., 110, 269
Mann, I., Grun, E., Wilck, M., et al. 1996, Icarus, 120, 399
Marchi, S., Morbidelli, A., & Cremonese, G. 2005, A&A, 431, 1123
Marzari, F., & Vanzani, V. 1994, A&A, 283, 275
Marzari, F., Scholl, H., Farinella, et al. 1996, Icarus, 119, 192
Mukai, T., & Yamamoto, T. 1982, A&A, 107, 97
Sykes, M. V., & Greenberg, R. 1986, Icarus, 65, 51
Sykes, M. V., Grün, E., Reach, W. T., et al. 2004, The Interplanetary Dust Complex and Comets, Comets II (Tucson: University of Arizona Press), 677
Wiegert, P. 2009, Icarus, 201, 295